Modeling of a Single Pulse Electric Discharge at Sphere/flat Interface by Coupling Contact Multiphysics and Phase Transformations

G. Maizza*, P. Di Napoli, and R. Cagliero
Politecnico di Torino. Dipartimento di Scienze dei Materiali ed Ingegneria Chimica.
*G. Maizza. Corso Duca degli Abruzzi, 24. 10139 Turin, Italy. Email: giovanni.maizza@polito.it

Abstract: Bulk and contact multiphysics is of great theoretical and technological interest to many engineering applications, such as spot welding, current-assisted powder metallurgy, electrical circuitry (switches), electrical motors, etc. A multifield model is developed with the aim of predicting material properties changes in a steel sample subjected to a high intensity dc pulse by two spherical electrode tips. Both bulk and contact multiphysical phenomena are analyzed along with the effects of non linear changes in the electrical, thermal and mechanical properties and phase transformations in the steel sample. The goal of this study is to predict the time dependent evolution of the coupled field phenomena in terms of (i) phases' progress (ii) phases' distribution (iii) physical and mechanical properties changes in the field-affected zone. To the authors' knowledge there are no previous attempts dealing with the transient solution of fully coupled electrical, thermal, mechanical and metallurgical phase fields in contact problems.

Keywords: contact, electrical, structural, thermal, welding.

1. Introduction

Capacitor discharge welding (CDW) is a DC pulsed process which combines short processing times (order of milliseconds) and high localized energy density to ensure rapid heating and cooling so that a wide range of metals, alloys, ceramics, composite and dissimilar materials can be welded with unique joints' property combinations of high strength and toughness.

Despite its recognized technological advantages and potentials (e.g. versatility, low energy consumption, throughput, automatization, low environmental impact) the CDW process is difficult to set-up in real practice as well as to diagnose and control during on-line processing owing to the rapid cycling, the occurrence of interacting fields and the very narrow heat affected region at the contact interface. The process set-up is especially difficult when dissimilar materials have to be welded and/or different (other than spherical) projections at the electrode tips are designed.

The actual CDW cycle consists of two basic steps: a) mechanical preloading under a constant imposed force; b) combined current pulse discharge and constant imposed force (identical to preloading's force). The process involves the interaction of mechanical, electrothermal and, in case of steel samples, also phase transformations on both heating and cooling. The rapid phase transformation on heating remarkably affects the final mechanical properties.

This work aims at improving our fundamental understanding behind the CDW process via a finite element modeling of the essential physical fields and inherent materials properties involved during one single dc-pulse heating in the case of a case-hardened steel sample and two spherically shaped Molybdenum electrodes. Due to the cylindrical geometry and the particular loading system an axial-symmetric model is formulated in the COMSOL Multiphysics package. Various built-in features and modules are invoked (i.e. the pair contact feature [1], the elasto-plastic solver [2], the DC-electrical solver [3] and the thermal solver [4], whereas the steel solid state transformations are modeled by user-defined functions. A new concept of materials' properties definition is proposed to account for the more realistic double dependence on temperature and phases content in steels.

2. The CDW process

Essentially, the CDW machine is based on a RLC electric circuit shown in Fig. 1. The primary circuit includes a high voltage supply and a capacitor bank. The secondary circuit is composed of two Mo electrodes and the steel sample to be pulse-heated. Both circuits are connected to each other with a transformer which transforms the primary high-voltage /low-intensity current into a secondary low-voltage/high intensity current. A power switch is used to close the RLC circuit upon current discharge.

The current impulse may be of up to 0.5 mega-ampere intensity and 5-20 ms.

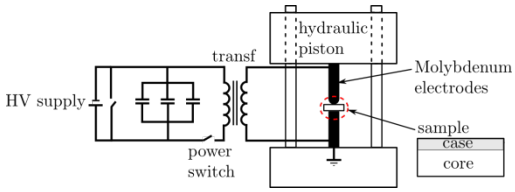

Figure 1. Schematics of the CDW device.

The force is applied to the electrodes by a hydraulic piston. This force does not change throughout either the preloading or the CDW cycle. It serves two main purposes, (i) ensure an intimate contact between the electrodes and the sample (ii) counterbalance the electro-magnetic forces which would misplace the joint upon discharging. The preloading force remarkably influences the discharge cycle as it affects the electrical, thermal and strain contact phenomena.

The employed steel sample is a standard case-hardened low-carbon steel (AISI 9310).

3. The CDW model

3.1 The model geometry

The CDW system domain is shown in Fig.2. The diameter and length of the electrodes are 10 mm and 30 mm. Its hemispherical tip diameter is 10 mm.

The steel sample is modeled as a bilayer composite having an upper martensitic layer (case) of eutectoid composition and a lower a annealed (i.e. ferrite-pearlite) layer (substrate) of 0.1% initial carbon content.

The thicknesses of the case and substrate layers are 0.6 mm and 9.4 mm respectively. The sample radius is assumed to be large enough so as end effects are negligible. Accordingly, due to the natural axial-symmetry of the CDW system only one quarter of it requires computation.

3.2 The mechanical model

The Mechanical Structural module [2] is involved in the overall model as stationary elasto-plastic problem in response to the imposed force by means of the electrodes. The electrode, the sample and the contact region are assumed to behave elasto-plastically, with the isotropic hardening formulated in terms of the tangent modulus E_{Tiso}. The high temperature elasto-plastic behavior is taken into account by the change of the local temperature and microstructure composition.

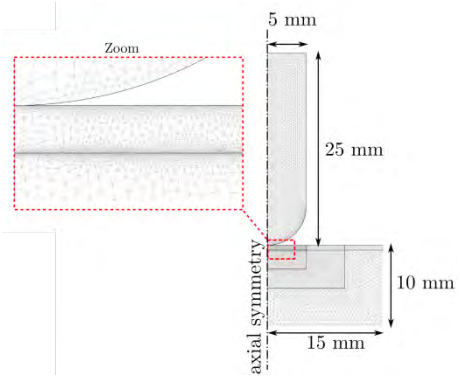

Figure 2. Geometry and mesh of the electrode-sample system.

The imposed boundary conditions are as follows: (a) constant force imposed at the upper surface of the electrode, (b) fixed displacement at the bottom surface of the sample c) free condition at the remaining boundaries.

Secion 3.6 will illustrate in detail how this model will be solved in time, coupled with the other fields, along the CDW cycle.

After the preloading stage the trasmitted pressure at the shaped electrode tip leaves a spherical indentation over the sample surface. The contact area rapidly evolves in time during the current discharge as a result of the combined elastic (by thermal expansion) and plastic strains. The instantaneous radius of the contact (or constriction) area a_c is the most important model's output used to couple the mechanical model to the electric model [6]. The mechanical properties (σ_y, E, E_{Tiso}) are additional key coupling factors due to their dependence on temperature and phase content.

3.3 The DC Electrical model

The electric field in the system domain is in general governed by the Maxwell's equations [5]. However, if we assume that the electromagnetic forces can be ignored, there are no conducting charges and no transient effects, the Maxwell's equations reduce to the well-known (stationary) Poisson equation:

$$\nabla \cdot (\sigma \nabla V) = 0 \tag{1}$$

where σ is bulk electrical conductivity and V is voltage. This field is managed by the AC/DC Electrical module. An important output of this module, other than the voltage (or current density) is the Joule heat distribution dissipated by the electric currents in the bulk and at the contact interface. The Joule heat per unit volume is given by:

$$\dot{Q}_T = \sigma(T)\,|\nabla V|^2 \tag{2}$$

This quantity is introduced as heat source term in the transient heat conduction equation.
The corresponding Joule heat at the contact interface is governed by the Holm's theory [6] which states that the contact resistance R_c of two mating bodies, whose electrical resistivities are denoted as ρ_{e1} and ρ_{e2}, is given by:

$$R_c = (\rho_{e1} + \rho_{e2})/r_c \tag{3}$$

where r_c is the radius of the contact area. From Eq.3 the calculation of effective contact conductivity (σ_c), required by the AC/DC Electric module, is straightforward. Note that this module employs a *virtual resistive layer* of *d* thickness to model a contact resistance. By definition, a contact resistance will cause a voltage drop (or current density discontinuity) across the two contacting bodies:

$$\mathbf{n} \cdot (\mathbf{J}_1 - \mathbf{J}_2) = \frac{\sigma_c}{d} (V_1 - V_2) \tag{4}$$

where **n** is unit vector normal to the interface, **J** is current density, and subscripts 1 and 2 denote either contacting surfaces.

3.4 The Thermal field

The thermal field descends from the electrical field. The temperature evolution in a conducting body is governed by:

$$\rho\, c_p\, \partial T/\partial t = \nabla(k \nabla T) + \dot{Q}_T \tag{5}$$

where ρ, c_p k and $\dot{Q}_T$ are density, specific heat, thermal conductivity, and heat source term per unit volume as given by Eq.2.
The vertical walls of the electrode and top surface of the sample are supposed to exchange heat by convection with still room air; the upper surface of the electrode and the lower surface of the sample are assumed to be at constant temperature to mimic the thermal coupling to highly massive copper tooling.
A suitable interface condition accounts for the thermal contact resistance at the interface between the electrode and the sample. The interface condition is similar to Eq.4 except for the contact thermal conductivity and the temperature in place of the contact electrical conductivity and the voltage respectively.

3.5 The Phase transformation model

The materials properties of the electrodes are only function of temperature.
Conversely, as the steel sample undergoes allotropic transformation on heating its materials properties are functions of both temperature and content micro-constituents (hereinafter, *phases*) such as austenite, which forms at high temperatures at the expense of the initial two phases, ferrite/pearlite (substrate) and martensite (case).
This feature allows to establish an intimate multiphysic coupling between all physical fields in both the bulk and at the contact provided that a suitable materials property model for steels is designed.

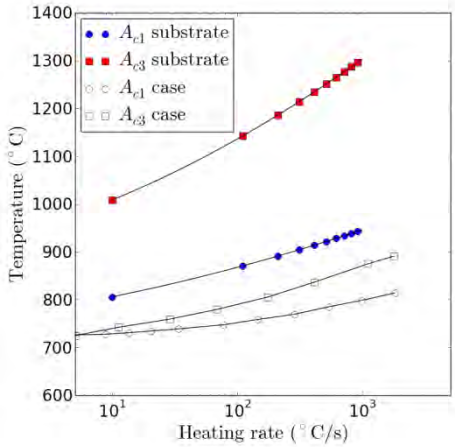

Figure 3. Ac1 and Ac3 temperatures vs heating rate for a low carbon (0.1%C) (substrate) and an eutectoid (0.7%C) steel (case).

To realistically model CDW on rapid heating, inertial effects on reaustenitization has to be taken into account.
These inertial effects influence both the initial A_{c1} and the final A_{c3} critical points. The change of these points with the heating rate is experimentally evaluated for the two given steels [7,8] as reported in Fig.3. Accordingly, the phase bounds are defined as follows:

$$F_{\mathrm{f/p}} = 1 \,:\, T \leq A_{c1}(\dot{T}) \tag{7}$$

$$F_{\mathrm{a}} = 1\,;\, T \geq A_{c3}(\dot{T}) \tag{8}$$

$$F_{\mathrm{f/p,a}} = 1 \,:\, A_{c1}(\dot{T}) < T < A_{c3}(\dot{T}) \tag{9}$$

where f/p and a denote ferrite/pearlite and austenite, respectively.
To predict the austenite growth during rapid heating an anisothermal kinetics is normally required. However, the specific problem at hand may benefit from a suitable simplifying assumption which is helpful to speed-up the calculations without significantly compromising the reliability of the model results. Indeed, owing to the: a) high temperature cycling, b) high heating rates, c) rapid reaustenitization inside a d) very narrow heat affected zone, a simple lever rule can suffice to predict the current austenite volume fraction

rather than calculate it by integrating a time consuming anisothermal kinetics. Thus, under this simplifying assumption only Eq. 9 has to be calculate.
As the two-phase region may introduce in each material property, abrupt temperature discontinuities at the two ends, during phase changes, which can be dramatic for solution convergence, a sigmoid interpolation is designed to smooth-out such discontinuities. Thus, the two-phase zone of Eq. 9 is described by a sigmoid (lever rule) function. Thus, the generic ψ_i material property function can be expressed as:

$$\Psi_i = \psi_{i,A_{c1}}\,(T \le A_{c1}) + \Psi_{i,A_{c3}}\,(T \ge A_{c3}) + \Psi_{i,A_{c1}A_{c3}}\,(Ac1 < T < A_{c3}) \qquad (10)$$

where subscript *i* stands for stress-strain (1), electrical (2) or thermal (3) properties.
Figure 4 (b), exemplifies the application of Eq. 10 in the case of a thermal property (ψ_3), e.g. the thermal conductivity *k*. The observed plateau just accounts for the inertial effects on heating in the given property.
A mixture rule is used to compute the local effective property in a two-phase region.

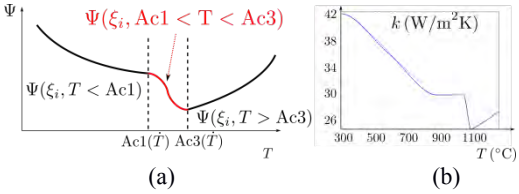

Figure 4. (a) Formulation of a generic property function Ψ vs temperature; (b) application to thermal conductivity property, *k*.

All materials properties are updated after completing the calculation of the thermal field. These are the made available to subsequent mechanical, electric and thermal prediction.

3.6 The field coupling strategy

The CDW multiphysics model is solved by coupling the aforementioned fields via an ad-hoc coupled solution strategy (see fig. 5). Efforts are made to implement the overall CDW model by the user interface to speed-up model set-up and error debugging.
Recall that, the electric, thermal, structural and metallurgical phase fields are coupled through the materials properties ψ_i and two coupling quantities, i.e. the dissipated heat source $\dot{Q}_T$ and the contact area a_c.
Figure 6 shows in more detail how the various fields interact to each other in time per a generic time step.

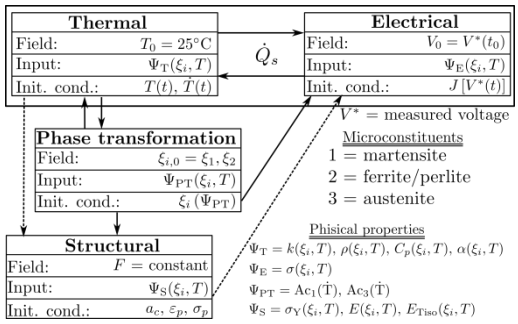

Figure 5. Multifield coupling strategy in the CDW model.

This figure contains two basic assumptions: a) the essential CDW phenomena are leaded by the temperature field; b) the time constant of electric phenomenon, is of the same order of magnitude of the thermal phenomenon. These two assumptions can be considered to be plausible if the time ranges of the measured voltage pulse and temperature pulse under the investigated process conditions are compared. Instrumented experiments show that these times are 35 and 80÷90 ms for the voltage and the temperature pulses respectively. As, the latter is recorded at the end of cooling, it turns out that electrical and thermal phenomena on heating, under the specified conditions, occur almost simultaneously. Note that, however, under different discharge conditions, i.e. voltage pulses much shorter than 35 ms, the above assumption might significantly deviate so as the full set of Maxwell's should be solved.

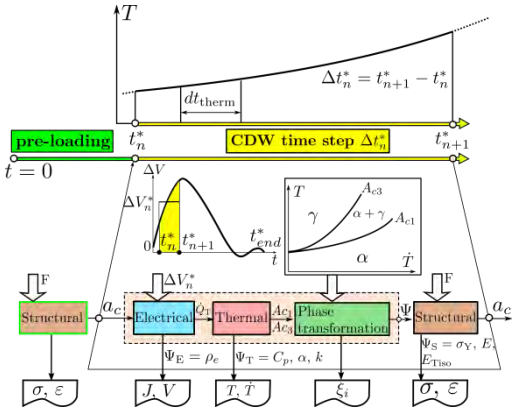

Figure 6. Schematics of the transient coupling strategy per generic time step.

At the instant t=0 the transient thermal field off-sets all fields so that they can march in time with a common *thermal* time. Fig. 6 shows the situation at the generic (thermal) time instant t_n^* and the generic time step Δt_n^* during the CDW heating. For completeness also the preloading cycle, (i.e. the stationary mechanical module), is shown. This module is

executed only ones, at t=0, to provide the initial contact area.
The force F (imposed at the upper electrode) is entered as input. The output of the stationary elasto-plastic model is in the effective (elastic and plastic) strain/stress field and, more importantly, the contact (or constriction) area underneath the electrode tip. This is used to subsequently couple the stress-strain field to the electric field. Initially, the mechanical properties are computed at room temperature and as a function of the initial microstructure composition.

In the generic CDW heating time step Δt_n^*, each field is sequentially executed starting with the stationary electric field. As the DC-Electric and Structural Mechanical modules are iteratively executed under the control of an external non-physical time parameter they can be viewed as *pseudo transient* solvers. Both solvers provides updated values of the ($\dot{Q}_T$, a_c) coupling quantities as output.
The first field to compute in the CDW cycle is the electric field. A voltage drop between the upper electrode and the sample edge is required to permit the calculation of a current flow across the joints by the stationary AC/DC Electric module. To this purpose a measured voltage-time pulse is introduced in the form of a discretized curve. This curve is defined over a time interval $0 \div t_{end}$. The internal time intervals are termed as *electrical time* intervals Δt^*.
For a generic electrical time interval Δt_n^* a corresponding constant value of the voltage drop can be extracted from the voltage-time curve. Knowing the input voltage drop, the electric field and the dissipated heat distribution ($\dot{Q}_T$) in the bulk and at the contact interface can be computed. With $\dot{Q}_T$ known the transient Heat Transfer module can be executed. This module takes trace of the CDW heating progress with a so called *thermal time*. While the *thermal* time coincides with *electric* time in the voltage-time curve, the *electrical* intervals Δt^* do not coincides with the *thermal* intervals. Generally the former is much larger than the latter. Each electrical time step can be selected by the user according to accuracy requirements. The width of the time interval affects the voltage drop value to be used in the AC/DC Electric module. The smaller are the time increments Δt^*, the more accurate is the electric field solution and thus the coupled field solution.
Thus, the integration in time of the thermal field makes the coupled field solution to also evolve in time with the same current thermal time. On the other hand, the thermal time step is usually automatically selected by the transient solver of the Heat Transfer module and thus much smaller than the electrical time step. According to Fig. 6, for the generic n^{th} thermal time t_n^*, the thermal solver will integrate the temperature field from t_{n-1}^* to $t_n^* = t_{n-1}^* + \Delta t_n$ using the voltage drop taken from the voltage-time curve at the same time t_n^*, defined over the corresponding time interval Δt_n^*.
The localized heat induces a rapid temperature increase and large temperature gradients across the interface. Depending on the local temperature and heating rate, the near contact region may undergo solid phase transformation (i.e. reaustenitization). The phase transformation model is illustrated in detail in next section. Worth to notice is that all materials properties are instantaneously compiled over the full temperature range, as a function of the local phase composition and the local heating rate.
The computed temperature and microstructure fields at t_n^*, will affect the stress-strain field, particularly the contact area, in the subsequent t_{n+1}^*.
In the following, the Comsol Multiphysics implementation will be described.

4. Implementation

4.1 Domain and mesh

The system is subdivided into three domains, the electrode, the steel core and the steel case. Specifically, the sample core and the sample case are considered as an assembly of 6 subdomains namely, 3 for the case and 3 for the core. This helps for mesh refinement.
The elements of the mesh are all triangular (advancing front) and they have the following dimensions: 1, 0.005 and 1 mm for the electrode, the case and the core, respectively. The contact boundary mesh sizes are set to 0.1 and 0.001 mm, respectively.

4.2 Structural

The two boundary conditions are: (1) applied load over the top face of the electrode, (i.e. pressure = 38.5 N/mm²) and (2) fixed displacement condition at the lower face of the core. A penalty factor p_n, is applied at the contact pair according to the manual [2] and an initial value of the contact pressure of 0.01 MPa to ensure good adhesion between the bodies.

4.3 Electrical

The voltage drop is applied with a constant potential value at the upper surface of the electrode and a ground condition at the lower

boundary of the sample core. All other boundaries are set as insulators. The electric interface condition is entered as a contact resistance condition, with a fictitious thickness value of 1 mm and the contact conductivity assumed as the reciprocal value of the sum of the two electrical resistivities.

4.4 Thermal

The initial temperature condition for the bodies is 25 °C. The electrode top surface boundary as well as the sample boundaries (lower face and side walls) are kept at room temperature. The vertical wall of the electrode and the top surface of the sample are assumed to exchange heat with the surrounding air, therefore subjected to a convective heat flux condition (heat transfer coefficient: 50 W/m^{2}K). The heat source term is calculated via the COMSOL variable `Qs_emdc`.

Phase transformation

Each material property is implemented according to Fig.4 and stored in individual data file.

The low and high temperature functions $\Psi_{A_{c1}}$ and $\Psi_{A_{c3}}$ are interpolating functions of the experimental property data [8-15]. The two-phase sigmoid function is calculated by the COMSOL `flc1hs` function [1].

4.5 Solvers' execution and setting

The UMFPACK is employed to solve both the stationary elasto-plastic and the time-dependent thermal models. The solution convergence of the former is accelerated with the augmented Lagrangian solver. The stationary contact mechanical model includes by default the contact pair boundary condition parameter `auglagiter`, which is included in the penalty factor expression. This parameter is incompatible with the thermal time-dependent solver [2]. Thus, to enable the coupling between the contact structural model and the thermal time-dependent model, the `auglagiter` parameter has been manually disabled after the former was executed.

This limitation imposes a non-automatic solution to be attained although the Comsol-user interface was chosen.

5. Results and discussion

The total preloading strains are shown in Fig.7. Three regions, corresponding to the electrode, the steel case and the steel core are clearly identified. The major total strain occurs at the core/case interface, with the core suffering higher strains than the upper case.

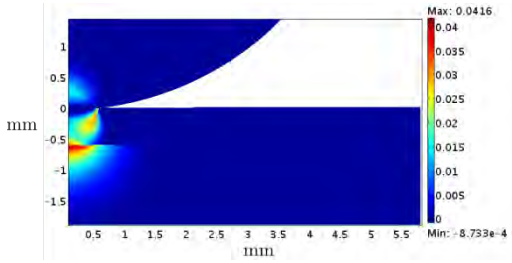

Figure 7. Total strains after preloading.

This is reasonable as the annealed core is much more ductile than the case hardened layer. However, high total strains are also observed at the electrode/case interface, although they are highly localized at the contact tip, suggesting a potential pile-up.

Figure 6 to 9 are related to the CDW cycle, showing combined mechanical, electro-thermal and metallurgical effects.

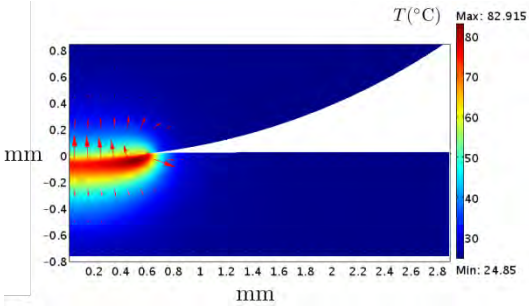

Figure 6. Temperature and total heat flux fields (arrows) after 0.2 ms (ΔV^*=1 V).

Figure 6 depicts the thermal field together with the total heat flux. The largest temperature gradients are observed at the case/electrode contact, especially at the surface of the steel case. The temperature peak of about 83 °C (0.2 ms) is found towards the contact tip, as a result of the highest contact resistance concentrated at the tip. The molybdenum electrode acts as a severe heat sink, due to its high thermal conductivity, thereby subtracting heat from the heat affected zone.

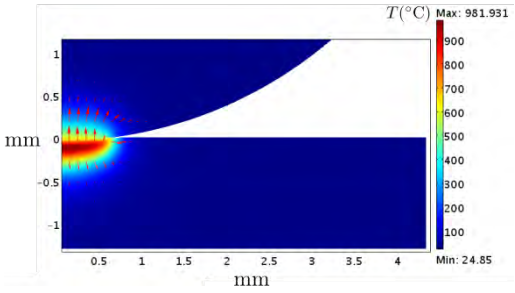

Figure 8. Temperature and total heat flux fields (arrows) after 3 ms (ΔV^*=3.05 V).

The heating effect corresponding to 3.05 V input voltage drop (3 ms) is shown in Fig.8. The maximum attained temperature is about

982 °C. At this temperature peak phase transformations are fully developed in the heat affected zone, as shown in Fig. 9. After 2.8 ms a small amount of austenite is formed. Austenite grows even further and extends after just 0.2 ms. The electrode heat sink also affects the austenite distribution. It is concentrated much below the steel surface.
From 0.2 to 3 ms, the temperature peak shifts towards the vertical symmetry axis due to the low thermal conductivity of the newly formed austenite.

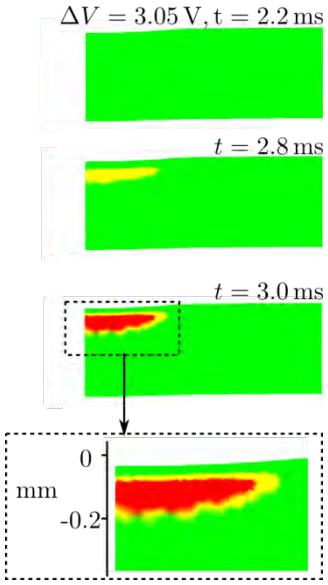

Figure 9. Austenite evolution vs time in the case hardened layer (green = martensite, yellow = martensite + austenite and red = austenite).

The intricate transient coupling between the electro-thermo-metallurgical field and the stress-strain field is better appreciated by the time variation of the contact area. Figure 10 compares the indentation depths for both the preloading and the discharge cycles. The latter corresponds to an imposed voltage of 2 V (2 ms). The largest depths (h) occur along the vertical axis although their values are relatively low due to the hardened case. The discharge cycle visibly contributes to a significant increase in local temperature in the heat affected zone. However, the resulting penetration depth after heating is larger but not remarkably higher than that attained after preloading. Even though the superficial case is very hard, the mechanical model accounts for a slight deformation underneath the pressing electrode. Worth to mention is the effect of the thickness of the virtual contact resistive layer on the temperature field.

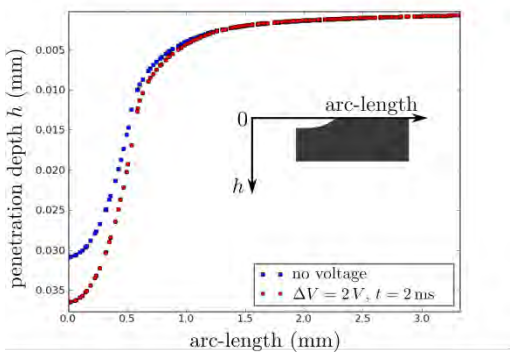

Figure 10. Penetration depth variation before and after the electrical discharge.

Special purpose simulations show that this parameter, despite its fictious purpose, impacts very dramatically on the temperature peak values, the extension and the distribution of the heat affected zone. More experiments are required to understand its actual physical meaning.
Convergence solution difficulties are encountered in the calculation of the structural mechanic field, especially when large strain gradients are involved. A mesh refinement in the most critical areas is envisioned to overcome this problem.

6. Conclusions

The intricate bulk and contact multiphysics of the CDW process has been successfully modeled by coupling in time the electrical, thermal, metallurgical and structural fields. A novel concept of material properties definition, in terms of temperature and phases (or temperature time derivative), has been introduced to take into account phase transformation on heating in the steel sample. The materials properties, the dissipated joule heat distribution and the contact area constitute the fundamental coupling factor between the involved fields. The designed coupling strategy is suitable for the general architecture and solvers of COMSOL Multiphysics 3.5a. Difficulties in the solution convergence are experienced in the calculation of the mechanical field, especially when large strain gradients are encountered. This occurs when approximately 900 °C peak temperature is reached in the heat affected zone.
The developed model is capable of capturing the essential multiphysics of the real CDW process, thus providing a useful computational tool to aiding understanding fundamental aspects of the process as well as to design experiments.

7.References

[1] COMSOL Multiphysics 3.5a: *User's guide*
[2] COMSOL Multiphysics 3.5a: *Structural Mechanics Module User's Guide*
[3] COMSOL Multiphysics 3.5a: *AC/DC Module User's Guide*
[4] COMSOL Multiphysics 3.5a: *Heat Transfer Module User's Guide*
[5] J. C. Maxwell, *A Treatise on Electricity And Magnetism.* Vols 1 and 2. (1904)
[6] R. Holm, *Electrical Contacts*, Hugo Gebers, Stockholm, (1936).
[7] J. Orlich, A. Rose and P. Wiest, Atlas Zur *Warmebehandlung der Stahle*, Band 3, Verlag Stahleisen M.B.H., Dusseldorf, (1973).
[8] J. Orlich, A. Rose and P. Wiest, Atlas Zur *Warmebehandlung der Stahle*, Band 4, Verlag Stahleisen M.B.H., Dusseldorf, (1974)
[9] W. Mitter, F.G. Rammerstorfer, O. Grundler, and G. Widner, *Discrepancies between calculated and measured residual stresses in quenched pure iron cylinder*, Mat. Sci. Tech., 1, 793-797 (1985).
[10] K.F. wang, S. Chandrasekar, and H.T.Y Yang, *Finite element simulation of induction heat treatment*, J. Mater. Eng.ng Perf., 1, 97-110 (1992)
[11] ASM Metals Reference Book, *Physical properties of carbon and alloy steels*, Ed. M. Bauccio, 3rd ed., (1997)
[12] P. Archambault, S. Denis, and A. Azim, *Inverse resolution of the heat-transfer equation with internal heat source*, J. mater. Eng.ng Perf., 6, 240-246 (1997).
[13] R. Schroder, *Thermal and residual stresses in quenched steel cylinders*, Mater. Sci. Tech., 1, 754-764 (1985)
[14] X. Uao, J. Gu, J. Li, and M. Hu, *Transient temeprature and internakl stress analysis of quenched centric and eccentric tubes*, Z. Metallkd. 94 60-66 (2003)
[15] C.H. Gur, A.E. Tekkaya, Mat. Sci. Eng.ng A319–321, 164–169 (2001)

8. Acknowledgements

The authors wish to express their sincere appreciation to Regione Piemonte (local government) – Direzione Regionale alle Attività Produttive - for funding the Green Engine for Air Traffic 2020 (Great 2020 - Ecoprolab) research project of Bando Regionale 24/12/2007 – Misura Ri.7 – Asse 1“Ricerca e Innovazione” – (LR 34/2004) which has allowed to develop the present research work. Also, the AVIO S.P.A. group (Rivalta – TO) and the AvioProp s.r.l. (NO) are deeply acknowledged for providing the mechanical data.